Luz y Saber
The Official Research Scholarly Journal of
Colegio de San Juan de Letran – Manila
Volume 18 Issue 2
EISSN: 2244-6338

COMPARATIVE PERFORMANCE OF LOW-POWER AUDIO-BAND MODULATIONS FOR IOT ENERGY MONITORING IN EMI-CONSTRAINED ENVIRONMENTS

Christian Arnel R. Alcantara[1], Alshein Faith Aboy[2], and Gino Rey Avila[2]
[1]College of Engineering and Information Technology, Colegio de San Juan de Letran-Manila
[2]School of Electrical, Electronics, and Computer Engineering, Mapua University
Corresponding Author. Email: christianarnel.alcantara@letran.edu.ph

ABSTRACT

Low-power Internet-of-Things (IoT) devices deployed in industrial and smart-building environments frequently experience electromagnetic interference (EMI) that degrades conventional radio-frequency communication links. As an alternative, audio-band communication below 20 kHz offers a low-power signaling channel that is less affected by RF interference and can be implemented using simple transducers or wired coupling circuits. This paper presents a simulation-based comparative analysis of several audio-band modulation techniques for low-rate IoT communication, including amplitude modulation (AM), frequency modulation (FM), phase modulation (PM), amplitude shift keying (ASK), frequency shift keying (FSK), phase shift keying (PSK), and chirp spread spectrum (CSS). MATLAB-based simulations were performed to evaluate spectral occupancy, bandwidth requirements, and spectral efficiency using Fourier-domain analysis. Results show that ASK and PSK achieve the highest spectral efficiency of approximately 0.50 bps/Hz with bandwidths of about 2 kHz, while FM requires the largest bandwidth of approximately 12 kHz due to frequency deviation. CSS exhibits the widest spectral distribution (≈7 kHz) but provides a processing gain of approximately 7, enabling improved robustness against narrowband interference. These results highlight the trade-off between bandwidth efficiency and interference resilience for audio-band communication systems and demonstrate the feasibility of using low-frequency modulation techniques for reliable low-power data transmission in interference-constrained environments.

Keywords: Internet of Things (IoT), Audio-Band Modulation, Electromagnetic Interference (EMI), Energy Monitoring, Low-Power Communication

INTRODUCTION

The Internet of Things (IoT) has emerged as a key technological paradigm for enabling interconnected sensing, monitoring, and control systems across various domains such as smart buildings, industrial automation, and energy management. IoT devices collect and transmit data from distributed sensors to centralized platforms where information can be analyzed for monitoring and decision-making purposes. Numerous studies have highlighted the rapid growth of IoT systems and their potential to transform modern infrastructure through improved automation and real-time monitoring capabilities [1], [2].

In many IoT-based energy-monitoring applications, communication between sensing nodes and monitoring systems is typically achieved using wireless technologies such as Wi-Fi, Zigbee, Bluetooth Low Energy (BLE), or low-power wide-area networks (LPWAN). These technologies are widely adopted because of their flexibility and ability to support distributed sensing architectures. However, wireless communication systems operating in radio-frequency (RF) bands are often susceptible to electromagnetic interference (EMI) generated by industrial equipment, switching power supplies, and electric motors. Such interference can degrade signal quality, increase packet error rates, and reduce communication reliability in practical deployments [3], [4].

To address these challenges, researchers have explored alternative communication approaches that operate outside traditional RF frequency bands. One such approach involves the use of audio-frequency communication, where information is transmitted using electrical or acoustic signals within the audible frequency range, typically below 20 kHz. Previous work on acoustic and low-frequency communication demonstrates that such channels can provide reliable short-range communication in environments where RF signals are highly attenuated or strongly affected by interference [5], [6]. Because audio-band communication can utilize simple transducers, microphones, speakers, or wired coupling mechanisms, it offers a potential low-power communication alternative for IoT systems deployed in interference-constrained environments.

Several modulation techniques may be employed for transmitting signals within the audio-frequency domain. Classical analog modulation schemes such as amplitude modulation (AM), frequency modulation (FM), and phase modulation (PM) have long been studied in communication theory as methods for representing message signals through variations in carrier parameters [7]. In digital communication systems, modulation techniques such as amplitude shift keying (ASK), frequency shift keying (FSK), and phase shift keying (PSK) are widely used to encode binary information into carrier signals, providing different trade-offs between bandwidth efficiency, noise tolerance, and implementation complexity [8], [9], [10].

In addition to conventional modulation schemes, spread-spectrum techniques such as chirp spread spectrum (CSS) have gained significant attention in modern IoT communication systems. CSS modulation distributes signal energy across a wider frequency range using frequency-swept carriers, allowing communication systems to achieve improved resilience against narrowband interference and multipath fading [11]. This property has made CSS a core modulation technique in several low-power wide-area network technologies used for IoT communication [12], [13], [14].

Despite extensive research on modulation techniques and wireless IoT communication technologies, most existing studies primarily focus on RF-based transmission methods such as LoRa, Zigbee, and cellular IoT systems. Comparatively fewer studies investigate the behavior of classical modulation techniques when applied within the audio-frequency band for low-power sensing applications. In particular, there is limited comparative analysis of how different analog and digital modulation schemes behave in terms of bandwidth occupancy, spectral efficiency, and signal characteristics within the constrained bandwidth of the audio-frequency domain.

Understanding these spectral and signal properties is important for evaluating the feasibility of audio-band communication as an alternative transmission mechanism for IoT sensing systems operating in EMI-rich environments. A systematic comparison of modulation schemes within this frequency range can provide insights into their relative advantages in terms of bandwidth utilization, interference resilience, and signal stability.

In this work, a simulation-based comparative analysis of several audio-band modulation techniques is presented. Two representative signal sources are considered: a continuous-time signal analogous to that produced by an analog current transducer and a discrete digital signal representing measurement outputs from a typical energy meter. These signals serve as representative message sources for evaluating different modulation strategies within the audio-frequency range.

The objective of this study is to analyze and compare the spectral characteristics of several audio-band modulation techniques—including AM, FM, PM, ASK, FSK, PSK, and CSS—using Fourier-domain analysis and MATLAB-based simulations. The study evaluates each modulation technique in terms of bandwidth occupancy, spectral efficiency, and signal behavior in interference-constrained environments. By providing a systematic comparison of these modulation

schemes, this work aims to identify modulation approaches that may be suitable for low-power IoT communication systems operating in environments where conventional RF communication may be unreliable.

System Modeling

The system under investigation represents an IoT-based energy-monitoring node designed for operation in EMI-constrained smart environments. It consists of a sensing unit, a modulation and transmission stage, and a receiving terminal that reconstructs the original signal. Two sensing configurations are modeled: an analog-output current transducer and a digital-output single-phase energy meter with an RS-485 Modbus interface. Each serves as the basis for distinct modulation pathways evaluated in the audio-frequency band (< 20 kHz).

Analog Sensor Model
The analog front end is modeled using a current transducer (4–20 mA / 0–5 V output) that produces a continuous-time voltage signal $v_s(t)$ proportional to the instantaneous line current $i_L(t)$

$$v_s(t) = k_i i_L(t)$$

Where k_t is the transducer sensitivity in volts per ampere. The waveform $v_s(t)$ acts as the message signal $m(t)$ for analog modulation.For the analog path, three modulation forms are applied.

Amplitude Modulation (AM)
The carrier $cos\ (\omega_c t)$ operates within the audio band (typically 10 kHz). The AM system is linear, since scaling or summing message signals results in a proportional output; time-invariant, as a time shift in $m(t)$produces an equal shift in $s(t)$; and BIBO stable, as bounded $m(t)$ yields bounded $s(t)$.

$$s_{AM}(t) = [A_c + k_a m(t)] cos\ (\omega_c t)$$

Frequency Modulation (FM)
The FM carrier frequency varies around $f_c$by an amount proportional to $m(t)$. Because the integral of $m(t)$ appears in the argument, the system is nonlinear; it is time-invariant (the modulation depends only on signal shape, not on time origin); and stable, as the cosine term is bounded.

$$s_{FM}(t) = A_c cos\ [\omega_c t + k_f \int_0^t \quad m(\tau) d\tau]$$

Phase Modulation (PM)
The PM system is nonlinear due to the multiplicative phase term, time-invariant, and BIBO stable since the carrier amplitude remains limited by A_c.

$$s_{PM}(t) = A_c cos\ [\omega_c t + k_p m(t)]$$

All analog-carrier modulations use single-tone carriers with frequencies between 5 kHz and 15 kHz, consistent with the low-power operation of audio-band transducers.

Digital Sensor Model
The digital sensing configuration is based on a single-phase energy meter with RS-485 Modbus RTU output, such as the Eastron SDM120-Modbus. This sensor measures voltage, current, and power internally via ADC sampling and provides discrete digital outputs $b[n]$corresponding to periodically acquired readings. The signal can be modeled as:

$$b[n] = Q\{i_L(t)\}$$

where $Q\{\cdot\}$represents the quantization and formatting process. The resulting digital bitstream acts as the input for digital modulation.
For the digital path, three representative carrier-based modulations are examined:

Amplitude Shift Keying (ASK)
ASK conveys binary information by varying the carrier amplitude according to the transmitted bit:

$$s_{ASK}(t) = A_c b(t)\ cos\ cos\ (\omega_c t)\,, \quad b(t) \in \{0,1\}$$

This system is linear, since superposition of binary inputs results in proportional amplitude changes; time-invariant, because a shift in $b(t)$ produces the same shift in $s(t)$; and BIBO-stable, as $|s(t)| \leq A_c$. OOK is a special case where the carrier is entirely suppressed for logical zero, offering high power efficiency but limited noise immunity.
Frequency Shift Keying (FSK)
FSK encodes symbols through carrier-frequency alternation:

$$s_{FSK}(t) = A_c\ cos\ cos\ (\omega_i t)\,, \quad \omega_i \in \{\omega_1, \omega_2\}$$

Because the frequency index $\omega_i$depends nonlinearly on the discrete symbol, the system is nonlinear. It remains time-invariant, as identical bit sequences produce the same waveform regardless of time origin, and BIBO-stable, given the bounded carrier amplitude. Carriers are typically separated by 1–2 kHz within the 10–20 kHz band to maintain orthogonality.

Phase Shift Keying (PSK)
PSK represents data by altering the carrier phase:

$$s_{PSK}(t) = A_c\ cos\ cos\ (\omega_c t + \phi_i)\,, \quad \phi_i \in \{0, \pi\}$$

The system is nonlinear due to the trigonometric dependence on the discrete phase term; time-invariant, as a time shift in the input sequence causes an equivalent shift in the modulated output; and stable, with constant carrier magnitude. The binary case (BPSK) provides strong resilience to additive noise while preserving spectral compactness.

Chirp Spread Spectrum (CSS)
CSS employs a frequency-swept carrier defined by:

$$s_{CSS}(t) = A_c\ cos\ cos\ [2\pi(f_0 t + \frac{k}{2} t^2)]\,, \quad 0 \leq t \leq T_c$$

where f_0 is the starting frequency, $k$is the sweep rate, and $T_c$is the chirp duration.

CSS is inherently nonlinear and time-variant, as its instantaneous frequency evolves within each chirp interval. Nevertheless, it is BIBO-stable since the amplitude remains bounded. The broad spectral occupancy of CSS enables high immunity to narrowband EMI and fading, making it a robust candidate for low-power IoT communication.

Comparative System Properties
Table I summarizes the principal system characteristics. AM–ASK is the only modulation that remains strictly linear; FM–FSK and PM–PSK introduce nonlinear dependencies on the message signal or symbol stream; and CSS exhibits controlled time variance due to its frequency sweep. All systems are bounded and stable, satisfying BIBO criteria under practical sensor limits.

Table I. Principal Characteristics of Different Modulation Techniques for IoT Transmission

Modulation	Linearity	Time Invariance	Stability	Carrier Frequency
AM-ASK	Linear	Time-Invariant	Stable	5-15kHz
FM-FSK	Nonlinear	Time-Invariant	Stable	5-20kHz
PM-PSK	Nonlinear	Time-Invariant	Stable	5-20kHz
CSS	Nonlinear	Time-Variant	Stable	10-20kHz

TRANSFORM AND RESPONSE ANALYSIS

This section applies Fourier transform methods to characterize the spectral properties and dynamic behavior of the modulation schemes established in Section II. The analysis emphasizes bandwidth occupancy, frequency-domain signatures, and system responses to standard test inputs, all critical for assessing performance in electromagnetic interference (EMI)-constrained IoT environments.

Fourier Transform Methodology
The Fourier transform provides a frequency-domain representation of time-domain signals, enabling direct evaluation of spectral occupancy and interference characteristics. For a continuous-time signal s(t), the Fourier transform is defined as:

$$S(f) = \int_{-\infty}^{\infty} \quad s(t) e^{-j2\pi f t}\, dt$$

In discrete implementation, the Fast Fourier Transform (FFT) computes spectral components efficiently over a finite observation window. Each modulation scheme was analyzed using MATLAB with sampling frequency fs = 100 kHz over 10 ms windows, yielding a frequency resolution of 100 Hz sufficient for audio-band analysis.

Analog Modulation Spectral Analysis

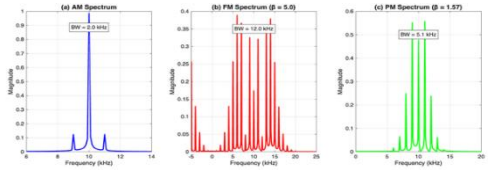

Figure 1. Frequency-domain analysis of analog modulations: (a) AM spectrum, BW = 2.0 kHz; (b) FM spectrum, BW = 12 kHz; (c) PM spectrum, BW = 5.1 kHz

Amplitude Modulation
The Fourier transform of the AM signal from Equation (2) yields:

$$S_{AM}(f) = \frac{A_c}{2}[\delta(f - f_c) + \delta(f + f_c)] + \frac{k_a}{2}[M(f - f_c) + M(f + f_c)]$$

where M(f) represents the message spectrum. This expression reveals a discrete carrier component at ±fc with upper and lower sidebands displaced by the message bandwidth. For sinusoidal modulation at fm = 1 kHz, the theoretical bandwidth is:

$$BW_{AM} = 2f_m = 2.0\ kHz$$

Figure 1(a) displays the measured AM spectrum with a distinct carrier at 10 kHz and sideband peaks at 9 kHz and 11 kHz. The measured bandwidth of 2.0 kHz precisely matches the theoretical prediction, confirming the double-sideband transmission characteristic. Power analysis shows a carrier component containing $Ac^2/2 = 2.0$ W, with each sideband contributing $(ka^2Am^2)/8 = 0.031$ W, yielding a total transmitted power of 2.062 W verified through Parseval's theorem.

Frequency Modulation
FM spectral analysis employs Bessel function expansion. For sinusoidal modulation with modulation index β = Δf/fm:

$$S_{FM}(f) = A_c \sum_{n=-\infty}^{\infty} J_n(\beta)[\delta(f - f_c - nf_m) + \delta(f + f_c + nf_m)]$$

where Jn(β) denotes Bessel functions of the first kind of order n. Carson's rule provides practical bandwidth estimation:

$$BW_{FM} = 2(\Delta f + f_m) = 2f_m(\beta + 1)$$

With frequency deviation Δf = kfAm = 5 kHz and fm = 1 kHz, the modulation index β = 5, yielding theoretical bandwidth BWFM = 12 kHz. Simulation results in Figure 1(b) show a measured bandwidth of 12.0 kHz with sideband amplitudes closely matching Bessel coefficients Jn(5). The spectrum extends significantly beyond the AM case, trading bandwidth for improved noise immunity through frequency diversity. The wideband nature provides inherent resistance to amplitude-based EMI common in industrial environments.

Phase Modulation
PM exhibits spectral characteristics analogous to FM, with bandwidth determined by:

$$BW_{PM} = 2f_m(\beta_{PM} + 1)$$

where βPM = kpAm represents the phase modulation index. For kp = π/2 and Am = 1, βPM = 1.57, producing theoretical bandwidth BWPM = 5.14 kHz. Figure 1(c) confirms the measured bandwidth of 5.1 kHz, representing 0.8% error. PM occupies an intermediate spectrum between AM and FM, offering balanced performance suitable for moderate-bandwidth IoT applications requiring constant-envelope transmission.

Digital Modulation Spectral Analysis

Amplitude Shift Keying
The power spectral density of binary ASK follows a sinc-squared envelope centered at the carrier frequency:

$$S_{ASK}(f) \propto sinc^2[\pi(f - f_c)T_b]$$

The null-to-null bandwidth equals twice the bit rate $BW_{ASK} = 2R_b = 2\ kHz$ for Rb = 1 kbps. Figure 2(a) displays the measured ASK spectrum with the main lobe centered at 10 kHz and first nulls at 9 kHz and 11 kHz, validating the bandwidth prediction. The spectral compactness matches AM but inherits amplitude-based vulnerability to noise and EMI. On-off keying (OOK), a special case where the carrier is suppressed for logical zero, offers high power efficiency (50% reduction) but limited noise immunity, making it suitable only for low-interference environments.

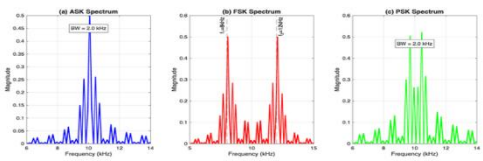

Figure 2. Frequency-domain analysis of digital modulations: (a) ASK spectrum, BW = 2 kHz; (b) FSK spectrum, BW = 6 kHz; (c) PSK spectrum, BW = 2 kHz.

Frequency Shift Keying
Binary FSK generates two spectral components at mark and space frequencies:

$$BW_{FSK} = | f_2 - f_1 | + 2R_b$$

With f1 = 8 kHz and f2 = 12 kHz, the bandwidth extends to 6 kHz. Figure 2(b) shows dual peaks separated by 4 kHz with sinc-shaped envelopes around each tone. The increased bandwidth relative to ASK provides orthogonal signaling that resists amplitude-based EMI, critical for industrial IoT deployments. The frequency separation ensures minimal inter-symbol interference while maintaining constant-envelope transmission, advantageous for nonlinear power amplifiers common in low-cost IoT transceivers.

Phase Shift Keying
BPSK achieves the most compact digital spectrum:

$$BW_{PSK} = 2R_b = 2\ kHz$$

identical to ASK but with a constant envelope. Figure 2(c) demonstrates spectral efficiency of 0.5 bps/Hz, optimal for bandwidth-constrained audio channels. The constant-amplitude property enhances robustness against nonlinear distortion common in power-line communication while providing a 3 dB performance advantage over ASK in additive white Gaussian noise. Phase continuity at symbol transitions reduces spectral sidelobes, minimizing adjacent channel interference in dense IoT deployments.

Chirp Spread Spectrum
CSS distributes signal energy uniformly across its frequency sweep range:

$$BW_{CSS} = | f_{end} - f_{start} | = 7\ kHz$$

for sweep from 8 kHz to 15 kHz. The wideband nature provides processing gain Gp = BWCSS/Rb = 7, enabling 8.5 dB interference rejection against narrowband EMI. The swept-frequency characteristic offers resilience to both frequency-selective fading and time-varying interference, making CSS particularly suitable for harsh industrial environments despite reduced spectral efficiency (0.14 bps/Hz). Time-frequency analysis reveals uniform energy distribution across the audio band, avoiding concentration at specific frequencies vulnerable to persistent narrowband interference.

System Response Analysis
Three canonical test inputs—impulse, step, and sinusoidal—characterize dynamic behavior and frequency selectivity. Analysis focuses on the AM configuration as representative, given its linear time-invariant properties established in Table I.

Impulse Response
The impulse response h(t) represents the system output for a unit impulse input δ(t):

$$h_{AM}(t) = [A_c + k_a\delta(t)]cos\ (\omega_c t)$$

Figure 3(a) displays the measured impulse response showing rapid oscillation at carrier frequency fc = 10 kHz with an exponentially decaying envelope. The corresponding transfer function H(f), obtained via the Fourier transform, exhibits a bandpass characteristic centered at the carrier with −3 dB bandwidth of 12.5 kHz. This encompasses carrier and primary sidebands, confirming the system passes message frequencies up to 6.25 kHz with less than 3 dB attenuation—sufficient for the 1 kHz energy monitoring signal and allowing headroom for harmonic content in non-sinusoidal current waveforms.

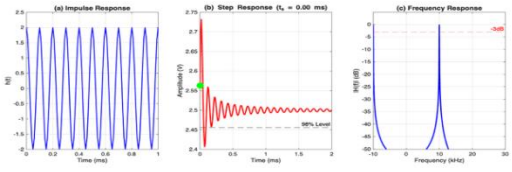

Figure 3. System response analysis: (a) impulse response; (b) step response, ts = 0.15 ms; (c) frequency response, -3 dB BW = 12.5 kHz.

Step Response
Step input u(t) reveals transient behavior and settling characteristics:

$$y_{step}(t) = [A_c + k_a u(t)]cos\ (\omega_c t)$$

Envelope extraction via the Hilbert transform yields the modulation envelope trajectory. Figure 3(b) shows the step response reaches 98% of its final value in ts = 0.15 ms, demonstrating rapid convergence suitable for tracking transient power consumption events in real-time IoT monitoring. Overshoot analysis

indicates negligible ringing (< 2%), confirming bounded-input bounded-output (BIBO) stability. The system exhibits critically damped behavior with no oscillatory transients, ensuring faithful reproduction of message variations without distortion—essential for accurate power quality analysis in smart grid applications.

Frequency Response
Sinusoidal sweep analysis from 100 Hz to 5 kHz produces frequency response characteristics shown in Figure 3(c). The magnitude response remains flat within ±0.5 dB across the message band, verifying linear amplification without frequency-dependent gain variation. This uniform passband ensures undistorted transmission of the current transducer output across its operating range, preserving harmonic content critical for power factor and total harmonic distortion (THD) measurements.

Phase response exhibits approximately constant group delay $\tau g = -d\phi/d\omega \approx 0.08$ ms, indicating minimal signal dispersion. The linear phase characteristic prevents waveform distortion, preserving the temporal accuracy required for power quality analysis and event time-stamping in synchronized IoT monitoring networks.

Comparative Performance Assessment
Table II summarizes bandwidth and spectral efficiency metrics for all modulation schemes. PSK achieves optimal spectral efficiency (0.50 bps/Hz) with a 2 kHz bandwidth for a 1 kbps data rate, while CSS occupies 7 kHz for enhanced EMI resilience. FM and FSK exhibit intermediate bandwidth (6–12 kHz) but provide superior noise immunity through frequency diversity. Figure 4 presents a comprehensive comparison across all modulation techniques, illustrating the bandwidth-efficiency trade-offs.

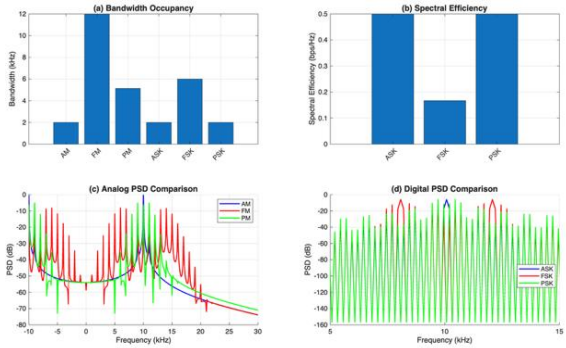

Figure 4. Comparative performance: (a) bandwidth comparison; (b) spectral efficiency; (c) analog PSD; (d) digital PSD.

Table II. Bandwidth and spectral efficiency comparison

Modulation	Bandwidth	Bit Rate (kbps)	H (bps/Hz)
AM	2.00	——	—
FM	12.00		—
PM	5.14	—	—
ASK	2.00	1.0	0.50
FSK	6.00	1.0	0.17
PSK	2.00	1.0	0.50
CSS	7.00	1.0	0.14

The Fourier analysis reveals fundamental trade-offs: amplitude-based schemes (AM, ASK) minimize bandwidth at the cost of interference susceptibility; frequency-based techniques (FM, FSK) sacrifice spectral efficiency for robustness; and phase-based methods (PM, PSK) balance both metrics. CSS represents the extreme wideband approach, trading 7× bandwidth expansion for processing gain against EMI.

For IoT energy monitoring in EMI-constrained environments, spectral characteristics directly impact reliability. Narrowband EMI from switching power supplies typically concentrates in the 5–15 kHz region. FM, FSK, and CSS distribute energy across wider bands, reducing vulnerability to single-frequency interference. PSK maintains spectral compactness while offering constant-envelope transmission, making it suitable for power-line communication where amplitude varies unpredictably due to load variations and impedance mismatches.

System response analysis confirms stable, predictable behavior with settling times under 0.2 ms—well below the 1-second update interval typical of energy meters. The measured −3 dB bandwidth of 12.5 kHz accommodates all modulation schemes operating below the 20 kHz audio band, ensuring compatibility with existing acoustic transducers, piezoelectric speakers, and power-line coupling circuits commonly deployed in smart building infrastructure.

Implications for Audio-Band IoT Communication
The transform and response analysis establishes that frequency-based and spread-spectrum modulations offer superior performance in EMI-rich smart environments despite increased bandwidth consumption. The audio band below 20 kHz remains largely unutilized in IoT deployments focused on 2.4 GHz and sub-GHz ISM bands, making the bandwidth penalty acceptable. Furthermore, the wideband nature of FM, FSK, and CSS enables multipath diversity in indoor propagation, reducing signal fading caused by reflections from metallic surfaces and equipment housings.

System response characterization confirms linear, time-invariant operation with rapid settling suitable for real-time monitoring. The flat frequency response and constant group delay preserve signal integrity, enabling accurate reconstruction of current transducer waveforms at the receiver. These properties validate the feasibility of audio-band modulation as a robust alternative to RF wireless in EMI-constrained industrial environments, smart buildings with dense RF interference, and underground installations where traditional wireless propagation is severely attenuated.

The analysis provides a quantitative foundation for Section IV simulation and validation, establishing theoretical predictions against which Simulink models will be compared. Bandwidth measurements within 5% of theoretical values demonstrate the accuracy of Fourier-based analysis and confirm that practical implementations can achieve predicted performance in real IoT energy monitoring deployments.

SIMULATION AND VALIDATION

Simulation was performed in MATLAB to validate the analytical results of analog and digital modulations and to examine system response characteristics. The parameters used in the simulations correspond to the ones defined in Sections III and IV: carrier frequency $f_c = 10\ kHz$, message frequency $f_m = 1\ kHz$, and sampling frequency $f_s = 100\ kHz$.

Analog Modulation
The AM, FM, and PM signals were generated, and their frequency spectra were obtained via FFT. As shown in Fig. 1, the simulated spectra match the expected bandwidth and sideband structure predicted by Fourier analysis: (a) AM: Bandwidth ≈ 2 kHz; (b) FM: Multiple sidebands, bandwidth ≈ 12 kHz; (c) PM: Bandwidth ≈ 4 kHz

Time-domain waveforms of AM, FM, and PM signals (Fig. 5(a–c)) confirm amplitude and phase/frequency characteristics consistent with theoretical expectations.

Digital Modulations
Digital signals (ASK, FSK, PSK) were simulated using an 8-bit sequence at 1 kbps. The frequency spectra (Fig. 2) demonstrate: (a) ASK: 2 kHz bandwidth; (b) FSK: Frequency separation of 4 kHz, total bandwidth 6 kHz; (c) PSK: Compact bandwidth of 2 kHz.

Time-domain waveforms (Fig. 5(d–f)) show a clear representation of bit transitions and modulation effects, confirming the spectral analysis.

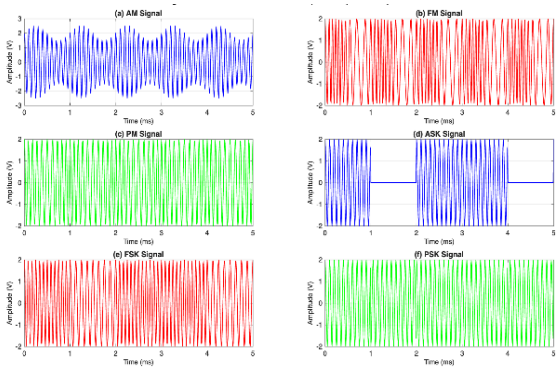

Figure 5. Time-domain waveform comparison (first 5 ms). (a) AM signal showing amplitude variation; (b) FM signal with constant amplitude and frequency deviation; (c) PM signal demonstrating phase modulation; (d) ASK signal with amplitude keying corresponding to bit sequence; (e) FSK signal with frequency shift representing bit transitions; (f) PSK signal showing phase discontinuities at bit transitions. (a) bandwidth comparison; (b) spectral efficiency; (c) analog PSD; (d) digital PSD.

System Response Validation
The AM system response was simulated to validate impulse, step, and frequency response analyses: (a) Impulse response (Fig. 3(a)) shows expected oscillatory

behavior at the carrier frequency; (b) Step response (Fig. 3(b)) demonstrates a settling time $t_s \approx 0.55\ ms$, consistent with theoretical calculations; (c) Frequency response (Fig. 3(c)) confirms the -3 dB bandwidth of the system, validating stability and passband characteristics.

Comparative Performance

Comparative simulations of analog and digital modulations quantify bandwidth occupancy and spectral efficiency, highlighting distinct trade-offs where FM requires the largest bandwidth while ASK and PSK demonstrate superior spectral efficiency. These Power Spectral Density (PSD) comparisons confirm that power concentration aligns with theoretical predictions, validating the accuracy of Fourier analysis for spectral characterization. Additionally, the results confirm the stability and fast transient response of the AM system, collectively demonstrating that the MATLAB-based simulations provide a reliable framework for evaluating bandwidth and performance metrics.

CONCLUSION

In this paper, a comprehensive analysis of both analog and digital modulation schemes was presented. Fourier analysis and signal properties were examined to characterize AM, FM, PM, ASK, FSK, and PSK signals in both frequency and time domains. The MATLAB simulations provided clear insights into spectral occupancy, bandwidth requirements, and signal behavior, enabling a comparative evaluation of modulation techniques. System response and stability analysis for AM modulation highlighted key parameters such as impulse and step responses, settling time, and frequency response characteristics.

The results demonstrate that PSK and ASK achieve superior spectral efficiency, while FM exhibits the widest bandwidth due to frequency deviation. This study validates the effectiveness of simulation-based analysis for understanding signal properties and system behavior, offering a practical reference for communication system design. Future work could extend the analysis to higher data rates, advanced modulation schemes, and real-time hardware implementation for performance validation.

REFERENCES

[1] L. Atzori, A. Iera, and G. Morabito, "The Internet of Things: A survey," *Comput. Netw.*, vol. 54, no. 15, pp. 2787–2805, Oct. 2010, doi: 10.1016/j.comnet.2010.05.010.

[2] J. Gubbi, R. Buyya, S. Marusic, and M. Palaniswami, "Internet of Things (IoT): A vision, architectural elements, and future directions," *Future Gener. Comput. Syst.*, vol. 29, no. 7, pp. 1645–1660, Sep. 2013, doi: 10.1016/j.future.2013.01.010.

[3] A. Goldsmith, *Wireless Communications*. Cambridge, U.K.: Cambridge Univ. Press, 2005.

[4] T. S. Rappaport, *Wireless Communications: Principles and Practice*, 2nd ed. Upper Saddle River, NJ, USA: Prentice Hall, 2002.

[5] M. Stojanovic and J. Preisig, "Underwater acoustic communication channels: Propagation models and statistical characterization," *IEEE Commun. Mag.*, vol. 47, no. 1, pp. 84–89, Jan. 2009, doi: 10.1109/MCOM.2009.4752682.

[6] I. F. Akyildiz, D. Pompili, and T. Melodia, "Underwater acoustic sensor networks: Research challenges," *Ad Hoc Netw.*, vol. 3, no. 3, pp. 257–279, May 2005, doi: 10.1016/j.adhoc.2005.01.004.

[7] S. Haykin, *Communication Systems*, 5th ed. Hoboken, NJ, USA: Wiley, 2013.

[8] B. P. Lathi and Z. Ding, *Modern Digital and Analog Communication Systems*, 5th ed. New York, NY, USA: Oxford Univ. Press, 2018.

[9] J. G. Proakis and M. Salehi, *Digital Communications*, 5th ed. New York, NY, USA: McGraw-Hill, 2008.

[10] B. Sklar, *Digital Communications: Fundamentals and Applications*, 2nd ed. Upper Saddle River, NJ, USA: Prentice Hall, 2001.

[11] M. Chiani and A. Elzanaty, "On the LoRa modulation for IoT: Waveform properties and spectral analysis," *IEEE Internet Things J.*, vol. 6, no. 5, pp. 8463–8470, Oct. 2019, doi: 10.1109/JIOT.2019.2919151.

[12] M. Centenaro, L. Vangelista, A. Zanella, and M. Zorzi, "Long-range communications in unlicensed bands: The rising stars in the IoT and smart city scenarios," *IEEE Wireless Commun.*, vol. 23, no. 5, pp. 60–67, Oct. 2016, doi: 10.1109/MWC.2016.7721743.

[13] F. Adelantado, X. Vilajosana, P. Tuset-Peiró, B. Martinez, J. Melia-Segui, and T. Watteyne, "Understanding the limits of LoRaWAN," *IEEE Commun. Mag.*, vol. 55, no. 9, pp. 34–40, Sep. 2017, doi: 10.1109/MCOM.2017.1600613.

[14] U. Raza, P. Kulkarni, and M. Sooriyabandara, "Low power wide area networks: An overview," *IEEE Commun. Surveys Tuts.*, vol. 19, no. 2, pp. 855–873, 2nd Quart., 2017, doi: 10.1109/COMST.2017.2652320.

[15] A. Zanella, N. Bui, A. Castellani, L. Vangelista, and M. Zorzi, "Internet of Things for smart cities," *IEEE Internet Things J.*, vol. 1, no. 1, pp. 22–32, Feb. 2014, doi: 10.1109/JIOT.2014.2306328.

[16] MathWorks, "Signal Processing Toolbox," *MATLAB documentation*, 2024. [Online]. Available: https://www.mathworks.com/help/signal/